THE JOURNAL OF PHYSICAL CHEMISTRY C

Article

pubs.acs.org/JPCC

Stark Spectroscopy of Absorption and Emission of Indoline Sensitizers: A Correlation with the Performance of Photovoltaic Cells

Nobuhiro Ohta,[*,†] Kamlesh Awasthi,[†] Kenji Okoshi,[‡] Kazuhiro Manseki,[§] Hidetoshi Miura,[∥] Yukiko Inoue,[∥] Kosuke Nakamura,[⊥] Hirohiko Kono,[*,⊥] and Eric Wei-Guang Diau[†]

[†]Department of Applied Chemistry and Institute of Molecular Science, National Chiao Tung University, 1001, Ta-Hsueh Road, Hsinchu 30010, Taiwan

[‡]Graduate School of Environmental Science, Hokkaido University, Sapporo 060-0810, Japan

[§]Graduate School of Engineering, Environmental and Renewable Energy System (ERES) Division, Gifu University, 1-1, Yanagido, Gifu 501-1193, Japan

[∥]R&D Center, Chemicrea Inc., 1-133 Ohtsurugi, Shimogawa Izumi-machi, Iwaki, Fukushima 971-8183, Japan

[⊥]Department of Chemistry, Graduate School of Science, Tohoku University, Sendai 980-8578, Japan

Supporting Information

ABSTRACT: Electric field effects on photoexcitation dynamics and electronic properties of highly efficient indoline sensitizers, DN488, D205, and DN182, embedded in PMMA films have been examined by using electroabsorption (E-A) and electrophotoluminescence (E-PL) spectroscopic techniques and time-resolved photoluminescence (PL) decay measurements in the presence of electric fields. Photovoltaic performances have been also measured for devices constructed using these sensitizers. Then, field-induced quenching of PL and field-induced change in PL decay profile were observed, and it was found that these field effects, which depend on the sensitizers investigated herein, are well correlated with the trend of power conversion efficiencies of the corresponding photovoltaic cells. Electric dipole moment and molecular polarizability of these sensitizers both in the ground state (S_0) and in the excited state have been calculated at the level of B3LYP/6-31G(d), and the differences of these physical parameters between S_0 and the excited state thus obtained have been compared with the ones determined from the E-A and E-PL spectra. The present study of Stark spectroscopy of indoline dyes provides new insights for the exciton dissociation property and carrier mobility of organic dyes, which are important factors to understand the operation mechanism in dye-sensitized solar cells.

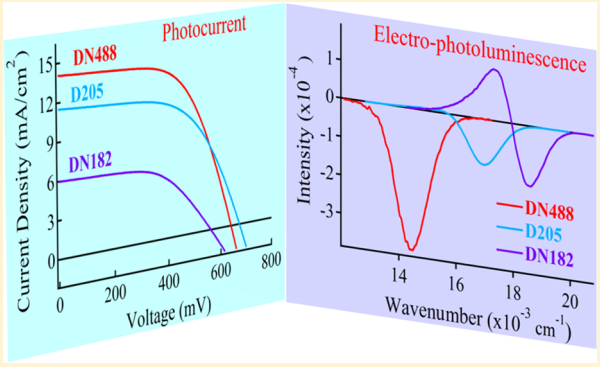

INTRODUCTION

Highly efficient photovoltaic devices have attracted tremendous attention as clean and environmentally friendly energy sources in the next generation to make a sustainable society. To achieve high efficiency, dye-sensitized solar cells (DSSCs),[1−5] organic bulk heterojunction solar cells,[6−9] quantum dot solar cells,[10−13] and recently perovskite solar cells[14−19] have been extensively studied.

The key issues to design and develop the photovoltaic devices which exhibit excellent performance are efficient carrier generation following photoexcitation of materials and efficient transportation of hole and electron in the bulk materials as well as in the interface between material and electrode. Such electronic properties and dynamics in excited states may be elucidated using electroabsorption (E-A) and electrophotoluminescence (E-PL) spectroscopic methods, where absorption and photoluminescence (PL) spectra are measured in both the absence and presence of an external electric field, because the charge-separated character in the excited state can be estimated from the electric dipole moment, based on the analysis of the E-A and E-PL spectra.

If the dissociation energy of exciton or hole−electron pairs is small, the dissociation may be easily induced by application of an external electric field, and exciton dissociation property as well as charge carrier mobility may be understood from the measurements of the field-induced change in PL spectra and decays. In fact, a good correlation between electric-field-induced fluorescence quenching and performance of photovoltaic devices was shown in DSSCs containing push−pull porphyrin dyes.[20] At present, the relation between electric field effect on PL spectra and decays and the performance of photovoltaic devices seems not to be realized well. Then further study may be necessary to confirm the relation between the performance of

Received: August 24, 2016
Revised: October 23, 2016
Published: October 24, 2016

DOI: 10.1021/acs.jpcc.6b08531
J. Phys. Chem. C 2016, 120, 26206−26216

photovoltaic devices and the electric field effect on absorption and PL spectra and PL decays.[21]

The elucidation of the effect of electric field on absorption and PL property seems to be also important from the viewpoint to understand the local field effects on materials in photovoltaic devices, since several authors stressed the local field effects on optical properties of DSSCs.[22−24] Furthermore, the working principle of photovoltaic cells may be elucidated based on the measurements of electric field effects on absorption and PL properties.

Indoline dyes are well-known as efficient metal-free organic sensitizers on titanium oxide (TiO_2).[25−29] In the present study, E-A and E-PL spectra of three color-tunable indoline dyes embedded in PMMA films were observed. The following three dyes were used: DN488, D205, and DN182 (Figure 1), i.e.,

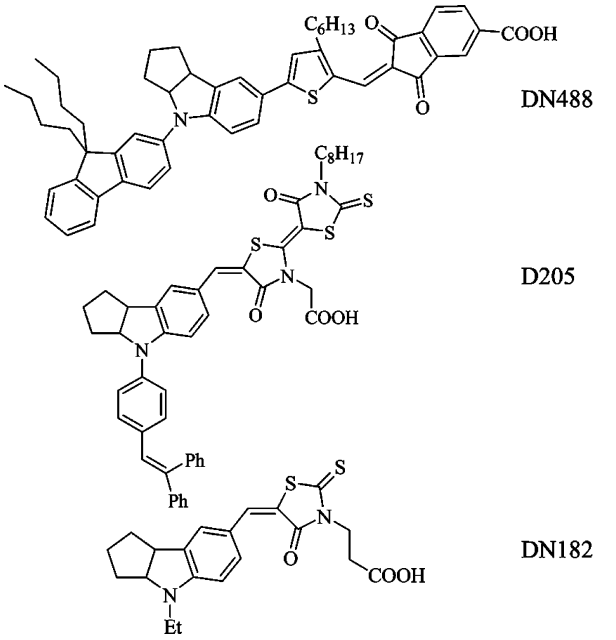

Figure 1. Molecular structure of indoline dyes of DN488, D205, and DN182 (from top to bottom).

2-{5-[4-(9,9-dibutyl-9h-fluoren-2-yl)-1,2,3,3a,4,8b-hexahydrocyclopenta[b]indol-7-yl]-3-hexyl-thiophen-2-ylmethylene}-1,3-dioxo-indan-5-carboxylic acid, 5-[[4-[4-(2,2-diphenylethenyl) phenyl]-1,2,3,3a,4,8b-hexahydrocyclopent[b]indol-7-yl]methylene]-2-(3-octyl-4-oxo-2-thioxo-5-thiazolidinylidene)-4-oxo-3-thiazolidineacetic acid, and 3-[5-(4-ethyl-1,2,3,3a,4,8b-hexahydrocyclopent[b]indol-7-yl)methylene]-4-oxo-2-thioxo-3-thiazolidinepropionic acid, respectively. D205 was synthesized with the same method as given in ref 26. The synthetic details of DN488 and DN182 are given in the Supporting Information. Based on the analysis of the observed E-A and E-PL spectra, we determined the magnitudes of the change in electric dipole moment and molecular polarizability following photoexciation and following emission. By using the density functional theory (DFT), the optimized molecular structures were determined, and the values of the electric dipole moment and molecular polarizability both in the ground state and in the excited state have been calculated. Based on the analysis of E-A and E-PL spectra and the DFT calculation, the electric dipole moment in the excited state as well as carrier generation from these indoline dyes attached to TiO_2 are discussed. The field-induced change in emission quantum yield has been determined from the observed E-PL spectra. Time-resolved emission decay profiles have also been measured in both the absence and presence of an electric field. Performance of photovoltaic cells constructed using these indoline dyes as sensitizers was also examined, and we found a good correlation between the performance of photovoltaic cells and the electric field effect on excitation dynamics of the sensitized dyes, i.e., on field-induced change in emission quantum yield as well as on emission decay profiles of the sensitized dyes. The relation between the electric dipole moment in the excited state and the performance of photovoltaic cells has been also discussed.

EXPERIMENTAL SECTION

Poly(methyl methacrylate) (PMMA, Aldrich, molecular weight 124 000−186 000) was purified by precipitation with a mixture of water and methanol. A certain amount of toluene solution of DN488, D205, and DN182 was cast on the indium−tin-oxide (ITO) coated quartz substrate by a spin-coating method. The concentration of each of the indoline dyes relative to the monomer unit of PMMA was 0.5 mol %. A semitransparent aluminum (Al) film was then deposited on the PMMA film, where indoline dyes were dispersed, by a vacuum vapor deposition technique. ITO and Al films were used as electrodes. The thicknesses of the PMMA films were determined with a thickness measurement system (NanoSpec/AFT model 010-0180, Nanomertrics). The typical thickness was ∼0.5 μm, and the applied electric field was estimated as the applied voltage divided by the thickness.

All the optical measurements were performed at room temperature. Steady-state absorption and PL spectra were recorded with an absorption spectrometer (HITACHI, U-3500, U-4000 or SHIMADZU, UV-1700) and a fluorescence spectrometer (JASCO, FP-777), respectively. Electric field modulation spectroscopy was applied to measure E-A and E-PL spectra, with the same apparatus as described elsewhere.[30,31] A modulation in transmitted light intensity of the excitation light (I_{EX}) and in PL intensity (I_{PL}) was induced by the application of the sinusoidal ac voltage with a modulation frequency of 40 Hz. Field-induced change in transmitted light intensity (ΔI_{EX}) or PL intensity (ΔI_{PL}) was detected with a lock-in amplifier at the second harmonic of the modulation frequency. The dc component of I_{EX} or I_{PL} was simultaneously observed. Note that the field-induced change in absorbance (ΔA) is given by $((2\sqrt{2}/\ln 10))\Delta I_{EX}/I_{EX}$, when $\Delta I_{EX} \ll I_{EX}$. E-A and E-PL spectra were obtained by plotting ΔA and ΔI_{PL}, respectively, as a function of wavelength or wavenumber. The angle between the direction of the applied electric field (**F**) and the electric vector of the excitation light was set to the magic angle (54.7°) in the E-A measurements, and depolarized emission was detected in the E-PL measurements.

Field-induced changes in PL decay profiles were also measured with a single-photon counting system combined with a pulse generator supplying a bipolar square wave.[32] A brief description of the decay measurements including a homemade equipment is given in Supporting Information.

The performance of photon-to-electric energy conversions was examined by fabricating dye-sensitized solar cells (DSSCs) in a similar manner to the one reported by Ito et al.[26] Plots of the current density as a function of voltage, i.e., $I-V$ curves, were obtained under AM 1.5 simulated sunlight (100 mW/cm^2) by using YAMASHITA DENSO CORPORATION YSS-80A. A black mask (4 mm × 5 mm) was used to regulate the active area of the device. Photocurrent action spectra, i.e., plots of the incident monochromatic photon-to-current conversion

DOI: 10.1021/acs.jpcc.6b08531
J. Phys. Chem. C 2016, 120, 26206−26216

efficiency (IPCE) as a function of excitation wavelength, were also obtained using a BUNKO-KEIKI CEP-2000 system.

The preparation of dye-sensitized nanocrystalline-TiO_2 and Pt electrodes was described elsewhere;[33] the thickness of the transparent nanocrystalline-TiO_2 layer (JGC C&C, PST-18NR) was ~8 μm, and the scattering layer was not used. For the dye uptake, the TiO_2 electrodes were immersed into the DN488, D205, and DN182 solution, respectively, with a concentration of 0.2 mM in a mixture of acetonitrile and *tert*-butylalcohol (v/v, 1:1) and kept at room temperature for 30 min or 6 h. For the coadsorption, chenodeoxycholic acid with a concentration of 0.4 mM was added. The dye-adsorbed TiO_2 electrode and Pt counter electrode were assembled into a sealed sandwich-type cell by heating with a hot-melt ionomer film. A drop of the electrolyte solution was placed on a drilled hole in the counter electrode of the assembled cell and driven into the cell by means of vacuum backfilling. The hole was then sealed with an additional hot-melt film and a cover glass. The electrolyte was composed of 0.1 M lithium iodide, 0.6 M 1,2-dimethyl-3-propylimidazolium iodide, 0.05 M I_2, and 0.05 M 4-*tert*-butylpyridine in 3-methoxypropionitrile.

RESULTS

E-A and E-PL Measurements. Absorption spectra of target molecules of indoline dyes DN488, D205, and DN182 observed in chloroform solution and in a PMMA film are shown in Figure 2. E-A spectra of DN488, D205, and DN182 doped in a PMMA film were observed with a field strength of 0.8 MV cm^{-1}. The results are shown in Figure 3, together with the absorption spectra and their first and second derivative spectra. In order to judge whether the field-induced change in PL intensity comes from the field-induced change in absorption intensity and/or the field-induced change in PL quantum yield, E-A measurements are absolutely necessary. Before the E-PL measurements, therefore, E-A measurements were done.

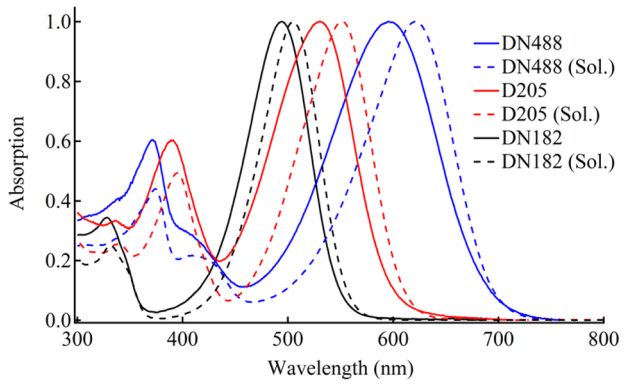

Figure 2. Absorption spectra of DN488, D205, and DN182 in PMMA (solid line) and in chloroform solution (broken line).

E-PL spectra of DN488, D205, and DN182 doped in a PMMA film were also observed with a field strength of 0.8 MV cm^{-1} and with excitation at 428, 400, and 458 nm, respectively. The results are shown in Figure 4, together with the PL spectra and their first and second derivative spectra. All the excitation wavelengths correspond to the ones where the field-induced change in absorption intensity was negligible (see Figure 3), and so the field-induced change in PL intensity is attributed to the change in emission quantum yield. As shown in Figure 5, the field-induced change in PL intensity (ΔI_{PL}) was proportional to the square of the applied field strength in every case.

The origin of the field-induced change in emission quantum yield can be determined by measuring the field-induced change in emission decay profile. If the population of the emitting state is influenced by **F**, the emission intensity at the initial stage of time following excitation should be affected by **F**. On the other hand, the emission lifetime should be shorter, if nonradiative decay or/and radiative decay is enhanced by **F** at the emitting state. Accordingly, the field-induced change in decay profile has been measured, and the results are shown in Figure 6. In this figure, we present the decay profiles of the time-resolved PL intensity at time t obtained at zero field ($I_0(t)$) and at 0.8 MV cm^{-1} ($I_F(t)$), the difference between these two decay profiles, ($I_F(t) - I_0(t)$), and the ratio between these two decays ($I_F(t)/I_0(t)$). In every compound, the magnitude of $I_F(t)/I_0(t)$ at $t = 0$ is less than unity, indicating that the field-dependent nonradiative process from the photoexcierd state competes with the relaxation to the emitting state; i.e., the population yield of the PL emitting state following photoexcitation is smaller than unity in the presence of **F**, as shown in the Supporting Information (Figure S1). A large quenching of PL was prominent in DN488, and the amount of the quenching at $t = 0$ following photoexcitation, which is known from the value of $I_F(t)/I_0(t)$ at $t = 0$, is in the order of DN488 > D205 > DN182. Note that the value of $I_F(t)/I_0(t)$ less than unity indicates quenching. The field-induced decrease of the PL lifetime is confirmed in DN488 since $I_F(t)/I_0(t)$ decreases as a function of t (Figure 6c of DN488). The PL lifetime of D205 also shows field-induced decrease (Figure 6c of D205), whereas the PL lifetime of DN182 slightly increases in the presence of **F** (Figure 6c of DN182). The decay profiles observed both in the absence and in the presence of **F** were simulated by assuming a bi- or triexponential decay, and the preexponential factor as well as the lifetime of each component are shown in Table 1, together with the average lifetime. It is noted that the very small change induced by application of electric field in lifetime and preexponential factor shown in Table 1 is essential to reproduce the field-induced change in decay profile as well as the difference and ratio between decay profiles observed at zero field and in the presence of electric field.

Performance of Dye-Sensitized Solar Cells. Photovoltaic properties of dye-sensitized solar cells based on the indoline dyes DN488, D205, and DN182 were examined to compare the performance among these indoline dyes under the same experimental conditions. Photocurrent voltage curves obtained for DSSCs using these dye sensitizers are shown in Figure 7. These results of the $I-V$ curves were obtained with the devices where dye sensitizers were deposited on the electrode through 30 min immersion in dye solution. The short-circuit photocurrent density (J_{sc}), open-circuit photovoltage (V_{oc}), fill factor (FF), and photon-to-electric energy conversion efficiencies (η) of the devices obtained in an iodine-based electrolyte are shown in Table 2. This table also shows the results obtained with the devices where dye sensitizers were deposited on the electrode through 6 h immersion in dye solution. The performance of the devices shows a systematic trend on J_{sc} with an order of DN488 > D205 > DN182, resulting in the same order as the energy conversion efficiency η. Especially, the value of J_{sc} as well as η is much higher in DN488 than the others. It is noted that not only J_{sc} but also V_{oc} is much smaller in DN182 deposited on TiO_2 electrode with 6 h immersion than the others, which also leads to less efficiency of the solar cell with DN182. Since each material, e.g., TiO_2 electrode in devices, was not optimized, the present photon-to-electricity conversion efficiency in D205 is lower than the one

DOI: 10.1021/acs.jpcc.6b08531
J. Phys. Chem. C 2016, 120, 26206−26216

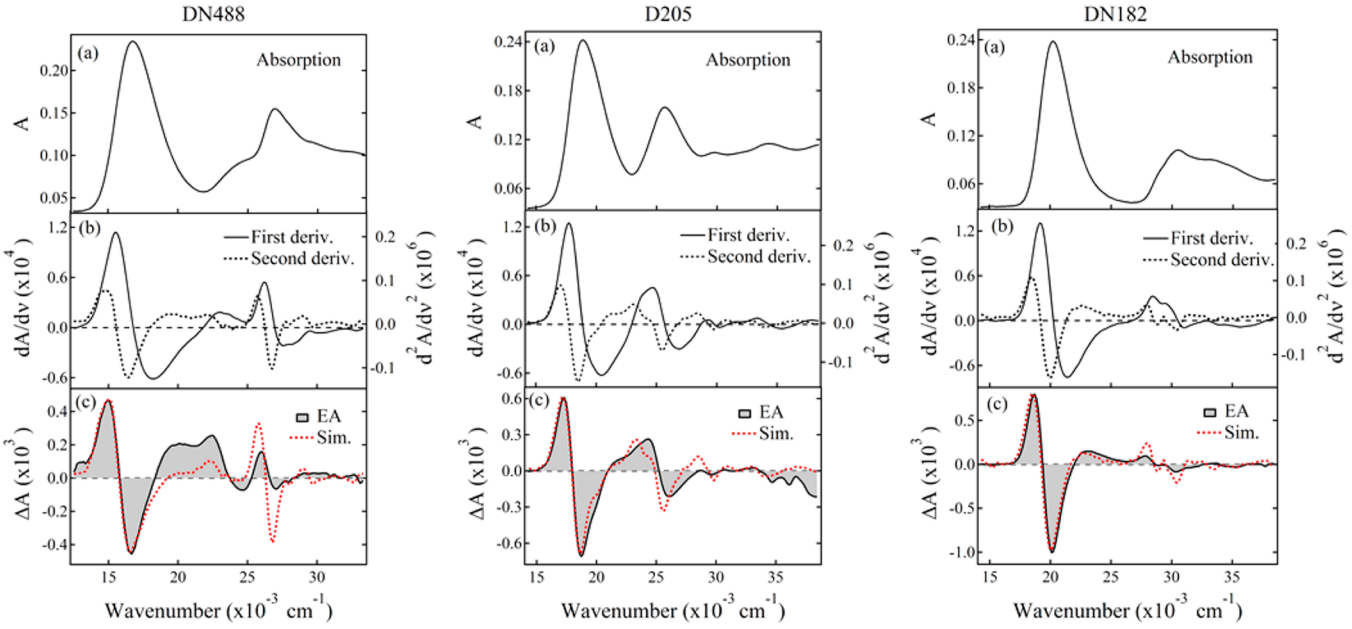

Figure 3. Absorption spectra (top), first and second derivatives of the absorption spectra (middle), and E-A spectra (bottom) of DN488, D205, and DN182 in a PMMA film (from left to right). The field strength was 0.8 MV cm^{-1}. Simulated E-A spectra are also shown in the bottom.

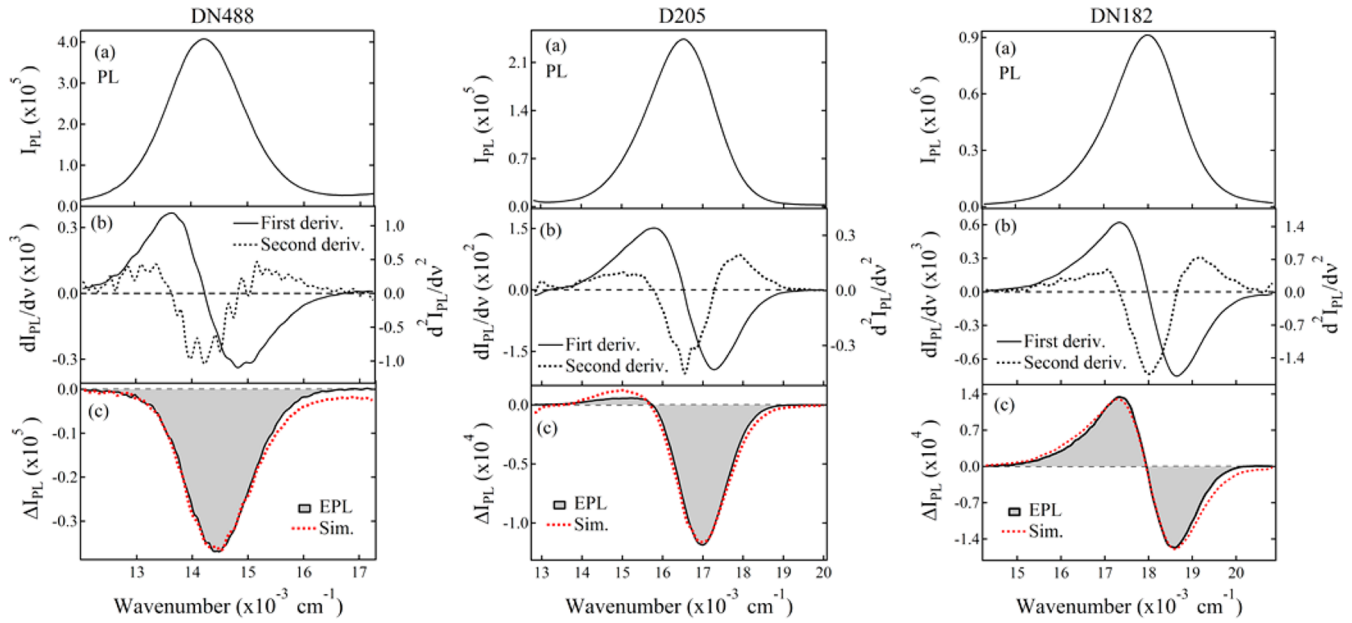

Figure 4. PL spectra (top), the first and second derivatives of the PL spectra (middle), and E-PL spectra (bottom) of DN488, D205, and DN182 in PMMA. The applied field strength was 0.8 MV cm^{-1}. Simulated E-PL spectra are also shown in the bottom.

reported so far.[26] However, the study of three indoline dyes makes it possible to fairly compare the device performance in order to understand the difference in efficiency using these dyes. The order of the overall photovoltaic performances obtained in the present experiments for DSSC constructed with the indoline dyes is considered to be consistent with the one of the optimized devices. The incident monochromatic photon-to-current conversion efficiency (IPCE), defined as the number of electrons generated by light divided by the number of incident photons,[34] was also obtained as a function of excitation wavelength with the devices where dye sensitizers were deposited on the electrode through 30 min immersion in dye solution. The results are shown in Figure 8. The absorption spectra of the devices used for the measurements of these IPCE spectra, i.e., for samples prepared with 30 min immersion of an electrode in dye solution, are shown in the Supporting Information (Figure S2).

Theoretical Calculation of Physical Parameters. We theoretically estimated the transition energy of the low-lying strong electronic absorption band and the electric dipole moments (μ) and molecular polarizabilities (α) of three dye molecules in the ground and excited electronic states by performing quantum chemistry calculations. D205 and DN488 dye molecules have long alkyl groups such as an *n*-octyl group, which results in many conformational isomers. For theoretical calculations, D205 and DN488 dye molecules were modeled by substitution of shorter alkyl groups for the long alkyl groups.

DOI: 10.1021/acs.jpcc.6b08531
J. Phys. Chem. C 2016, 120, 26206−26216

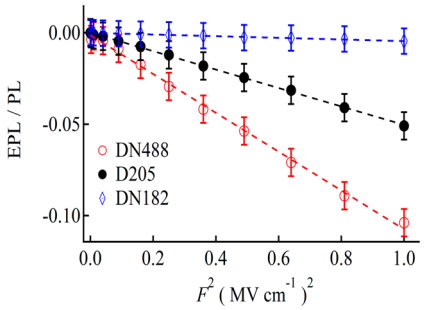

Figure 5. Plots of the field-induced change in PL intensity of DN488, D205, and DN182 in a PMMA film as a function of the applied field strength.

For D205, the *n*-octyl group was replaced by an ethyl group. For DN488, *n*-hexyl and *n*-butyl groups were replaced by an ethyl group and a methyl group, respectively.

The geometry optimization by DFT calculations was carried out with Gaussian 09, Revision A.02.[35] We employed the functional B3LYP, and the basis set we used was 6-31G(d).[36] The solvent effect of chloroform was considered by using the polarizable continuum model. The optimized geometries, confirmed by normal-mode analysis with the same program, are shown in the Supporting Information.

We calculated the values of μ and α and electronic transition energy at the optimized geometries. The molecules were rotated in the Cartesian space so that the polarizability tensor is diagonal. Roughly speaking, the long axis of the molecule is parallel to the *x*-axis. The values of μ and α in the ground state (S_0) obtained in the calculation are shown in Table 3. As shown in the Supporting Information (Figure S3), the dipole moment in S_0 is calculated to be in the order of DN182 > D205 > DN488. The peak positions of the main absorption bands are calculated by TD-B3LYP to be 462.10, 549.27, and 597.66 nm in DN182, D205, and DN488, respectively, which reproduce the observed peaks fairly well, i.e., 505, 552, and 621 nm, respectively, in chloroform solution. These absorption bands mainly come from the HOMO−LUMO transition. The isodensity surface plots of these HOMO and LUMO are shown in the Supporting Information (Figure S4). The HOMOs of DN488 and D205 are localized mainly at indoline groups, while the LUMOs are localized at the carboxylated 1,3-indandione group in DN488 and at the propionated thiazolidine group in D205. These results show that electron transfer from the indoline group to the 1,3-indandione group or thiazolidine group occurs nearly along the *x* axis (along the long axis) following excitation into the excited state, resulting in the large dipole moment along the long axis in the excited state.

We calculated the energies E_n of excited electronic states $\{n\}$ in the presence of a static electric field **F** and fitted the field-induced change of E_n, i.e., ΔE_n, to the form of $-\mu\mathbf{F} - \alpha\mathbf{F}^2/2$. The optimized values of dipole moments μ and polarizabilities α for the first excited state, to which the absorption intensity is very strong, are shown in Table 3, together with the values in S_0. The vector of μ in the excited state of each molecule is also shown in Figure 9, together with molecular structure, where the magnitude of μ can be compared easily among different molecules. It is found that the magnitude of μ is largely enhanced by excitation in DN488 and D205, and the magnitude of μ in the excited state is shown to be the order of DN488 > D205 > DN182 (Table 3 and Figure 9), in contrast with the ground state.

DISCUSSION

When an electric field, **F**, is applied to molecules, each energy level is shifted by $-\mu\mathbf{F} - \alpha\mathbf{F}^2/2$, as mentioned above. Due to

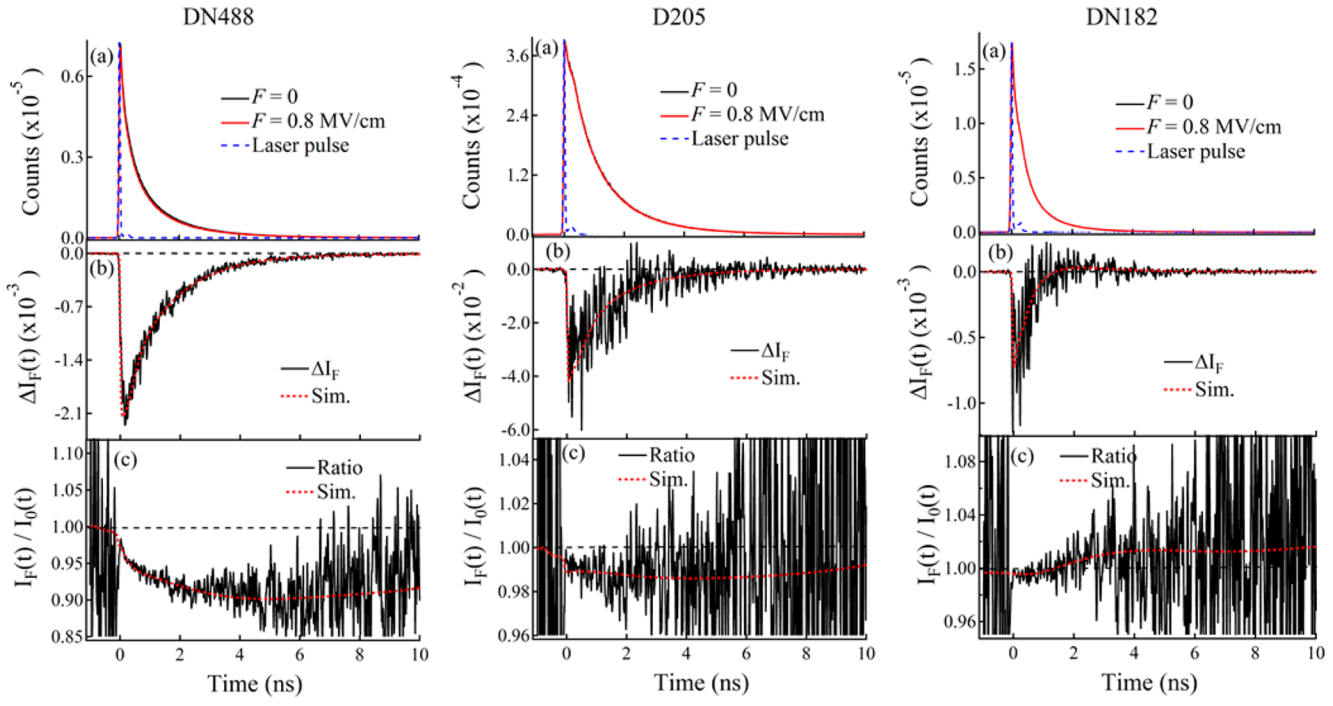

Figure 6. Electric field effects on PL decays of DN488 (left), D205 (middle), and DN182 (right) in a PMMA film: (a) Decay profiles at zero field and in the presence of an electric field; (b) the difference of the decay profiles observed at zero field and in the presence of electric field, i.e., $\Delta I_F(t)$ (= $I_F(t) - I_0(t)$); (c) the ratio between the decay in the presence of **F** relative to the decay at zero field, i.e., $I_F(t)/I_0(t)$. The applied field strength was 0.8 MV cm^{-1}. Simulated curves are also shown in (b) and (c).

DOI: 10.1021/acs.jpcc.6b08531
J. Phys. Chem. C 2016, 120, 26206−26216

Table 1. Results of the Analysis of the Fluorescence Decay Profiles of DN488, D205, and DN182 in PMMA Observed at Zero Field (OFF) and in the Presence of Electric Field of 0.8 MV cm^{-1} (ON)[a]

sample	electric field	τ_{av} (ns)	τ_{I} (ns)	τ_{II} (ns)	τ_{III} (ns)
DN488	OFF	0.588	0.197 (0.636)	1.138 (0.338)	3.000 (0.026)
	ON	0.565	0.192 (0.629)	1.110 (0.320)	2.890 (0.026)
D205	OFF	1.024	0.650 (0.680)	1.820 (0.320)	0
	ON	1.023	0.649 (0.670)	1.820 (0.315)	0
DN182	OFF	0.398	0.242 (0.770)	0.850 (0.216)	2.010 (0.014)
	ON	0.399	0.242 (0.766)	0.860 (0.212)	2.030 (0.014)

[a]Lifetimes of the different decaying components, i.e., τ_{I}, τ_{II}, and τ_{III}, are shown, together with the pre-exponential factor given in parentheses and the average lifetime, τ_{av}. Standard error in lifetime and pre-exponential factor is estimated to be ±5% with different samples, and the error of the average lifetime is roughly estimated to be ±10%. The results of the simulation which gives the best fit for each decay profile are shown in the table, not the average of the decay analysis.

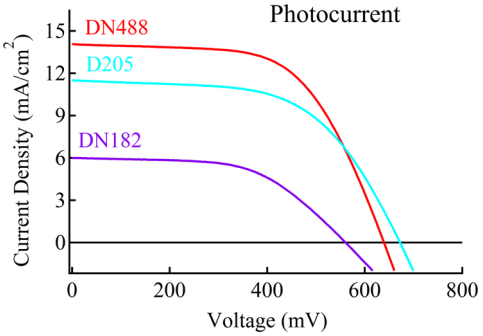

Figure 7. I–V curves of photovoltaic cells using DN488, D205, and DN182.

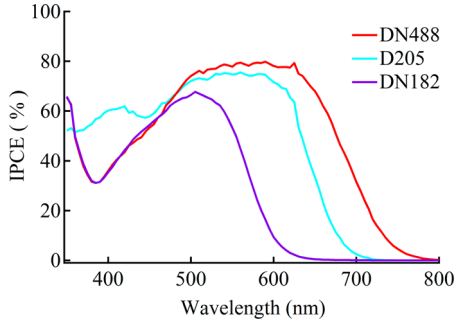

Figure 8. Photocurrent action spectra for TiO_2 films coated with DN488, D205, and DN182, respectively. Sensitized dyes were prepared by immersing TiO_2 electrodes to dye solution for 30 min. The incident photon-to-current conversion efficiency is plotted as a function of excitation wavelength. The IPCE values are not corrected for the loss of light intensity due to absorption and reflection by the conducting glass support.

the level shift, optical transition energy is shifted by $-\Delta\mu\mathbf{F} - \Delta\alpha\mathbf{F}^2/2$, where $\Delta\mu$ and $\Delta\alpha$ are the differences in electric dipole moment and molecular polarizability, respectively, between S_0 (μ_g and α_g) and excited state (μ_e and α_e), i.e., $\Delta\mu = \mu_e - \mu_g$ and $\Delta\alpha = \alpha_e - \alpha_g$. According to the theory of electric field effects on optical spectra, the field-induced changes in absorbance and PL intensity at wavenumber ν, i.e., $\Delta A(\nu)$ and $\Delta I_{PL}(\nu)$, are given by a linear combination of the zeroth, first, and second derivatives of the absorbance $A(\nu)$ and PL intensity $I_{PL}(\nu)$[37−42]

$$\Delta A(\nu) = (fF)^2\left[A_\chi A(\nu) + B_\chi \nu \frac{d}{d\nu}\left\{\frac{A(\nu)}{\nu}\right\} + C_\chi \nu \frac{d^2}{d\nu^2}\left\{\frac{A(\nu)}{\nu}\right\}\right] \quad (1)$$

and

$$\Delta I_{PL}(\nu) = (fF)^2\left[A'_\chi I_{PL}(\nu) + B'_\chi \nu^3 \frac{d}{d\nu}\left\{\frac{I_{PL}(\nu)}{\nu^3}\right\} + C'_\chi \nu^3 \frac{d^2}{d\nu^2}\left\{\frac{I_{PL}(\nu)}{\nu^3}\right\}\right] \quad (2)$$

Here f represents the internal field factor, and $F = |\mathbf{F}|$. When molecules are randomly distributed under the immobilized condition, the zeroth derivative coefficients A_χ and A'_χ originate from the field-induced change in absorption intensity and emission intensity, respectively. The coefficients of the first and second derivative components, i.e., B_χ (B'_χ) and C_χ (C'_χ), correspond to the spectral shift and broadening, respectively, of the E-A and E-PL spectra, which mainly come from $\Delta\alpha$ and $\Delta\mu$, respectively. These coefficients depend on the angle, χ, between the direction of the applied electric field and the electric vector of the excitation light or emission light. With the magic angle of χ (= 54.7°), the coefficients B_χ and C_χ are expressed as follows

$$B_\chi = \frac{\Delta\bar{\alpha}}{2h}, \quad C_\chi = \frac{|\Delta\mu|^2}{6h^2} \quad (3)$$

where h represents Planck's constant. $\Delta\bar{\alpha}$ denotes the trace of $\Delta\bar{\alpha}$, i.e., $\Delta\bar{\alpha} = (1/3)\,\mathrm{Tr}(\Delta\alpha)$. B'_χ and C'_χ are similarly given with the above equation. Then, the values of $\Delta\bar{\alpha}$ and $|\Delta\mu|$ can be

Table 2. Photovoltaic Properties of Devices with DN488, D205, and DN182 as Sensitizers on TiO_2 Thin Films under 1 sun Irradiation[a]

sample	J_{sc} (mA/cm^2)	V_{OC} (mV)	FF	η (%)
DN488	13.8 ± 0.3 (16.1)	645 ± 5 (625)	0.60 ± 0.02 (0.63)	5.34 ± 0.07 (6.34)
D205	12.1 ± 0.6 (12.7)	677 ± 7 (641)	0.57 ± 0.03 (0.63)	4.67 ± 0.38 (5.13)
DN182	6.3 ± 0.3 (10.4)	645 ± 5 (553)	0.56 ± 0.01 (0.63)	2.28 ± 0.39 (3.62)

[a]The average is shown with three devices where TiO_2 electrodes were immersed for 30 min in dye solution. The results with the devices where immersion was done for 6 h are given in parentheses, as a reference.

DOI: 10.1021/acs.jpcc.6b08531
J. Phys. Chem. C 2016, 120, 26206−26216

Table 3. Electric Dipole Moment (μ_x, μ_y, and μ_z in Units of Debye) and Molecular Polarizability (α_{xx}, α_{yy}, and α_{zz} in Units of Å^3) in S_0 and Excited State of DN488, D205, and DN182 Calculated at the B3LYP/6-31G(d) Level[a]

parameter	DN488	D205	DN182
	Ground State (S0)		
μ_x	6.72	9.29	12.36
μ_y	6.06	5.07	0.28
μ_z	−1.37	0.63	2.19
$\lvert\mu\rvert$	9.15	10.60	12.56
α_{xx}	228.74	241.78	116.88
α_{yy}	99.08	114.26	48.93
α_{zz}	49.09	52.36	26.79
$\bar{\alpha}$	125.64	136.13	64.20
	Excited State		
μ_x	34.69	31.01	18.57
μ_y	5.87	5.56	0.47
μ_z	−2.78	0.45	2.23
$\lvert\mu\rvert$	35.30	31.51	18.70
α_{xx}	609.78	1147.91	177.29
α_{yy}	123.60	160.54	51.08
α_{zz}	51.27	53.45	26.78
$\bar{\alpha}$	261.55	453.97	85.05

[a]The average values, i.e., $\lvert\mu\rvert$ and $\bar{\alpha}$, are also given.

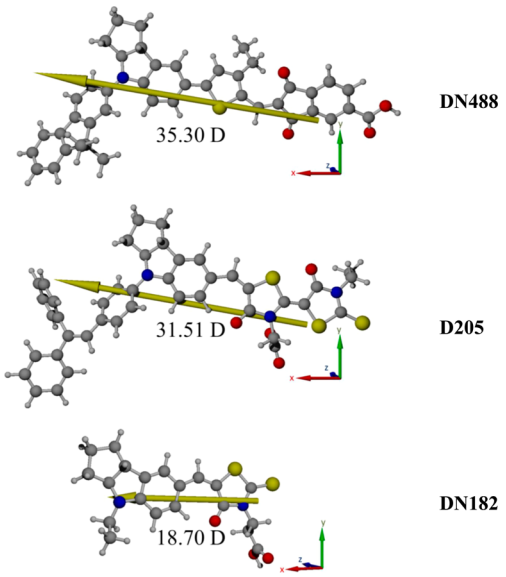

Figure 9. Electric dipole moment in the excited state of DN488, D205, and DN182 (from top to bottom) calculated at the B3LYP/6-31G(d) level.

obtained with eq 3, i.e., from the first and second derivative components of the E-A and E-PL spectra, respectively.

The zeroth derivative term of the E-A spectra comes from the field-induced change in transition moment, as far as molecules are fixed in the presence of **F**. Even when transition moment for emission is affected by **F**, the zeroth derivative term of the E-PL spectra does not always change. This is clearly understood by considering the case where any nonradiative process is nonexistent in the emitting state. In such a case, the emission quantum yield is unity irrespective of the presence of **F**, and emission intensity remains the same, as far as the absorption intensity is the same, though the emission decay profile, that is, the emission lifetime, is affected by **F**. From the zeroth derivative component in the E-PL spectra, accordingly, the field-induced change in emission quantum yield can be evaluated. Note that the field-induced change in emission quantum yield results from the change of the relation between radiative and nonradiative rate constants; that is, the field-induced change in radiative decay rate and nonradiative decay rate can be evaluated from E-PL spectra and time-resolved E-PL decays.

The analysis of the E-A spectra was done with attention to the lowest strong absorption band, and the simulated spectra are shown in Figure 3. The observed spectra were fitted by a linear combination of the first and second derivatives of the absorption spectra, and the zeroth derivative component was not necessary to be considered in the simulation, indicating that the field-induced change in intensity of the lowest absorption band is negligible. From the contribution of the first and second derivative components, the magnitudes of $\lvert\Delta\mu\rvert$ and $\Delta\bar{\alpha}$ following absorption to the lowest absorption band were obtained, based on eq 3. The results are shown in Table 4, together with the values of $\lvert\Delta\mu\rvert$ and $\Delta\bar{\alpha}$ determined from the theoretical calculation.

As in the case of the E-A spectra, E-PL spectra were simulated by a linear combination of the zeoth, first, and second derivative components of the PL spectra (see eq 2). In fact, the E-PL spectra of these compounds could be reproduced well by a linear combination of the zeroth, first, and second derivatives of the E-PL spectra, as shown in Figure 4. The observed E-PL spectra clearly show that the shape of the E-PL spectra of DN488 is very similar to the PL spectrum, indicating that the PL of DN488 is efficiently quenched by **F**. In comparison with DN488 or D205, the first and/or second derivative components are found to be very large in DN182. From each derivative component in the simulated spectra, the magnitudes of $\lvert\Delta\mu\rvert$ and $\Delta\bar{\alpha}$ following the emission process as well as the field-induced change in PL intensity were obtained. The results are shown in

Table 4. Magnitudes of the Changes in Electric Dipole Moment and Molecular Polarizability between S_0 and the Excited State Determined from the Analysis of the E-A and E-PL Spectra, Along with the Calculated Ones (Calcd)[a]

parameter		DN488	D205	DN182
$\lvert\Delta\mu\rvert$ (D)	E-A	14.7 ± 2.0	16.3 ± 2.0	18.2 ± 3.0
	E-PL	13.5 ± 1.5	12.9 ± 1.5	7.1 ± 1.0
	calcd	28.0	21.7	6.2
$\Delta\bar{\alpha}$ (Å^3)	E-A	156 ± 20	112 ± 10	106 ± 10
	E-PL	223 ± 20	2733 ± 200	1813 ± 200
	calcd	136	318	21
$\Delta I_F/I_F$ (%)		−7.1 ± 2.0	−2.9 ± 1.0	−0.30 ± 0.1

[a]The magnitudes of the field-induced change in fluorescence intensity at a field strength of 0.8 MV cm^{-1} relative to the fluorescence intensity at zero field, i.e., $\Delta I_F/I_F$, are also shown. The internal field factor is assumed to be unity in the E-A and E-PL measurements.

DOI: 10.1021/acs.jpcc.6b08531
J. Phys. Chem. C 2016, 120, 26206−26216

Table 4. The value of $|\Delta\mu|$ determined from the E-PL spectra is roughly the same as the one determined from the E-A spectra, though the order of $|\Delta\mu|$ among these molecules is reversed. In contrast with $|\Delta\mu|$, the magnitude of $\Delta\bar{\alpha}$ determined from the E-PL spectrum is much larger than that determined from the E-A spectrum in every molecule.

The values of $|\Delta\mu|$ and $\Delta\bar{\alpha}$ estimated from the theoretical values given in Table 3 are shown in Table 4, together with the values determined from the E-A and E-PL spectra. The order of $|\Delta\mu|$ among the molecules is the same as the one determined from the E-PL spectra, that is, in the order of DN488 > D205 > DN182. However, the calculated values of $|\Delta\mu|$ are much larger than the experimental values, except for DN182, even though the experimental values shown in Table 4 were obtained by assuming that the internal field factor was unity. Also the order of the values of $|\Delta\mu|$ obtained from the E-A spectra is not the same as the calculated one. There is a possibility that these indoline dyes did not take an optimized structure in PMMA films, while the calculation of $|\Delta\mu|$ was done for the optimized geometry. The disagreement of the order of $|\Delta\mu|$ among these molecules between experiment (E-A) and calculation may come from the restricted structure in PMMA. In the preparation of the photovoltaic devices, sensitized dyes were slowly deposited on the TiO_2 electrodes; i.e., it takes 30 min or more for deposition after immersing the electrode into dye solution. In such a slow deposition process, sensitized dyes are considered to attach on the surface with their optimized structure. On the other hand, the samples used for E-A and E-PL measurements were prepared by a spin-coating method, and polymer films which include dyes were coated on ITO electrodes in an instant. Then, indoline dyes used for the E-A and E-PL measurements may have been embedded in polymer films with unoptimized structures. The emitting state is produced by relaxation from the photoexcited state. During this process, structural change of molecules may occur in PMMA to take an optimized structure. Because of such a structural change, the order of the values of $|\Delta\mu|$ determined from the E-PL spectra may be the same as the calculated one. If we consider the structural change during the relaxation process to the emitting state, the large values of $\Delta\bar{\alpha}$ evaluated from the E-PL spectra may be interpreted; that is, the large values of $\Delta\bar{\alpha}$ may result from the orientational polarizability.[39,43] The most remarkable difference among the E-PL spectra of these molecules is the amount of the zeroth derivative component included in the E-PL spectra; i.e., the field-induced change in PL intensity is very different from each other. As shown in Table 4, the magnitude of the field-induced quenching, i.e., $|\Delta I_F/I_F|$, is the largest in DN488 and then the second largest in D205, while the field-induced quenching is very small in DN182.

Since the excitation in the E-PL measurements was done at the wavelengths where the field-induced change in absorption intensity was negligible, the field-induced quenching results from the field-induced decrease of the fluorescence quantum yield, as already mentioned.[31,44] The fact that the total absorption intensity of the lowest absorption band is not affected by **F** indicates that the radiative decay rate is not affected by **F**. As the origin of the field-induced change in emission quantum yield, therefore, the following two possibilities can be considered: (1) the nonradiative decay rate at the emitting state is affected by **F**; (2) the population yield of the emitting state following photoexcitation is affected by **F**. The measurements of the PL decay profiles in the presence and absence of electric field can solve the above problem.

PL decay profiles show that the value of $I_F(t)/I_0(t)$ at $t = 0$ is less than unity in all the dyes of DN488, D205, and DN182 (see Figure 6), indicating that the nonradiative process from the photoexcited state to the states other than the emitting state is affected by **F**. Probably, the exciton dissociation occurs directly from the photoexcited state in the presence of **F** in these indoline dyes (see Figure S1). The fact that the value of $I_F(t)/I_0(t)$ at $t = 0$ is much smaller in DN488 than in D205 or DN182 suggests that electron−hole pairs can be easily generated in DN488 from the photoexcited state. Also the field-induced shortening of the PL lifetime in DN488 implies that exciton dissociation easily occurs from the PL emitting state in the presence of eternal fields in competition with the emitting process. These results indicate that DN488 works more efficiently as a dye sensitizer of DSSCs than the others. In fact, DN488 shows the best performance among the photovoltaic cells constructed with DN488, D205, and DN182, respectively (see Figure 7 and Table 2). The field-induced quenching of PL of D205 is smaller than that of DN488 but more efficient than that of DN182. D205 also shows the field-induced shortening of the PL lifetime, whereas the PL lifetime of DN182 becomes longer in the presence of **F**. In the results, the performance of DSSC constructed with D205 is much better than that with DN182.

In efficient photovoltaic cells, the generation of electron−hole pairs which have small dissociation energy in the excited state may be essential. Accordingly the magnitude of μ in the excited state may be important in the sense that a large electric dipole moment is essentially the same as a pair of electron and hole separated at a long distance, where electrostatic attractive interaction is small. Then, the correlation between the photovoltaic performance and the electric dipole moment in the excited state has been examined, and it is found that the values of μ calculated for the excited state show a strong correlation with the performance of DSSC; that is, DN488 gives the largest value of $|\mu|$, while DN182 gives the smallest $|\mu|$, as shown in Table 3 and Figure 9, though it should be confessed that there is some discrepancy regarding $\Delta\mu$ between the calculated value and the value estimated from E-A or E-PL spectra. Note that DN488 and DN182 show the highest and lowest performance in solar cell, respectively (see Table 2).

As shown in Table 2, V_{oc} in the device prepared by 6 h immersion is much smaller in DSSC with DN182 than the others. Regarding the origin of the difference in V_{oc}, the following possibilities can be considered: (1) the energy level of TiO_2 film is shifted by attaching the DN182 molecules, resulting in the small difference between the Fermi level of TiO_2 and the redox potential of I^-/I_3^-; (2) carrier recombination between electrons injected into TiO_2 and I_3^- in electrolyte depends on the molecular size of sensitized dyes because the molecular length of DN182 is shorter than the others and I_3^- can easily approach to the TiO_2 surface in DN182, resulting in the enhancement of charge recombination; (3) the DN182-attached TiO_2 surface shows an easier carrier recombination with I_3^- because of the surface characterization such as the local field effect. Since DN488, D205, and DN182 give a similar V_{oc} in devices prepared by 30 min immersion, it is unlikely that the change in the Fermi level by attaching DN182 is very different from the one with attaching DN488 or D205. When the immersion time is long enough, it is likely that I_3^- can approach easily to the TiO_2 surface attached by DN182, resulting in the efficient carrier recombination, in comparison with two other dyes. The molecular length of DN182 is much shorter than the others (see Figure 1), and

DOI: 10.1021/acs.jpcc.6b08531
J. Phys. Chem. C 2016, 120, 26206−26216

indoline dyes are assumed to be attached perpendicular to the TiO_2 surface, when the immersion time of the electrode is long enough. In the results, the difference of V_{oc} between DN182 and others, observed with a long immersion time, may come from the difference of the molecular length, resulting in the efficient carrier recombination of electrons in TiO_2 with holes in I_3^-.

As the origin of the difference of J_{sc} among the indoline sensitizers in photovoltaic cells, the following two factors may be important: the collection efficiency of irradiation light and the efficiency of carrier generation, i.e., the efficiency of the electron injection from photoexcited sensitizers to TiO_2. As shown in Figure 2, the absorption peaks of DN488, D205, and DN182 are at 621, 552, and 505 nm in chloroform and 595, 531, and 494 nm in PMMA, respectively, indicating that the absorption spectrum extends to the longer wavelength region in this order. The light-harvesting efficiency of photovoltaic devices can be estimated from the overlap between the absorption spectrum of devices and incident light intensity distribution. The fact that the absorption spectrum of DN488 extends to a much longer wavelength region than the others implies the highest collection efficiency of the light in DN488 among these three dyes. On the other hand, E-PL spectra as well as field-induced changes in PL decay profile suggest another reason for the high photoenergy conversion in the photovoltaic cells constructed with DN488. Remarkable field-induced quenching of PL of DN488 shows that nonradiative relaxation process(es) following photoexcitation are enhanced by application of **F** in DN488. The relaxation process of these dyes which is affected by **F** may be regarded as the field-induced exciton dissociation which produces a hole and electron pair because a good correlation exists between the photon energy conversion efficiency of the photovoltaic cells constructed with these dyes and the magnitude of the field-induced quenching, as in the case of push−pull porphyrin dyes attached on TiO_2.[20] In other words, the dye which shows efficient field-induced exciton dissociation is regarded as a dye sensitizer suitable for DSSC.

The IPCE spectra given in Figure 8 show that the difference in photon energy conversion of the devices with these sensitized dyes comes not only from the difference in light-harvesting efficiency but also from the difference in electron-injection efficiency. As shown in the Supporting Information (Figure S2), the absorption spectra of the devices used for the measurements of these IPCE spectra give absorbance of more than two at wavelengths in the region of 510−550 nm in DN488 and D205 and at 480−490 nm in DN182; that is, more than 99% of the incident light is absorbed by devices in these wavelength regions. The IPCE in this excitation wavelength region gives the largest one in DN488, the next largest one in D205, and the next value in DN182. These results clearly show that the electron injection efficiency gives the same order with the one of the total photon energy conversion efficiency, i.e., DN488 > D205 > DN182.

Another difference among these molecules is the direction of the carboxylate group, which is bound to TiO_2 in the photovoltaic cell, relative to the direction of the dipole moment in the excited state, and the distance between the carboxylate group and electron-rich groups is different. As shown in Figure 9, for example, the carboxylate group of DN488 is attached to the indandione group with the same direction as the electric dipole moment, i.e., more or less along the x axis, while the carboxylate group in D205 and DN182 is bound to the thiazolidine group with very different direction from that of the x axis. The carboxylate group in DN488 is located near the electron-rich group (see Figure 9), in comparison with the carboxylate group in DN182, which is located far from the electron-rich group. It is therefore suggested that the electron injection from indoline dyes into the conduction band of TiO_2 to which dyes are attached is most favorable in DN488 and next favorable in D205, while the electron injection is not so favorable in DN182. Further, it is likely that the large electric dipole moment in the excited state enhances the electron injection from dye sensitizers to the TiO_2 surface in DN488. Thus, the difference in efficiency of the electron injection from sensitized dye molecules to TiO_2 is also one of the reasons why DN488, D205, and DN182 show very different performances from each other in photovoltaic devices.

CONCLUSION

We have measured E-A and E-PL spectra of indoline dyes of DN488, D205, and DN182 embedded in a PMMA film. E-PL spectra of these molecules show field-induced quenching of PL, and the field-induced quenching is especially prominent in DN488 and in the order DN488 > D205 > DN182. Time-resolved PL decay measurements show that field-induced quenching occurs immediately after photoexcitation, indicating that the nonradiative decay process, which is probably exciton dissociation enhanced by applied electric field, occurs from the photoexcited state. The lifetimes of PL of DN488 and D205 decrease in the presence of **F**, suggesting that field-induced dissociation occurs also from the emitting state of PL in these two molecules. In contrast, PL lifetime of DN182 was a little prolonged by application of electric fields, suggesting that exciton dissociation does not occur easily from the emitting state of PL in DN182 even in the presence of **F**. The device performances of DSSC constructed with DN488, D205, and DN182 have been also determined. The J_{sc} as well as the overall device performances show a systematic order DN488 > D205 > DN182. The order of the power conversion efficiencies is well correlated with the field-induced quenching, which is assignable to the field-induced exciton dissociation leading to the carrier generation. The present study demonstrated that the electric field effects on photoluminescence can be well correlated with the performances of photovoltaic devices.

The differences in electric dipole moment and molecular polarizability between S_0 and the lowest photoexcited singlet excited state and between the emitting state of PL and S_0 determined from the analysis of the E-A and E-PL spectra, respectively, have been compared with the ones calculated at the B3LYP/6-31G(d) level for the optimized structure. The order of the power conversion efficiency agrees with the order of the calculated electric dipole moment in the excited state, implying that the large charge-separated character of the excited state is important for high power conversion efficiency of DSSC.

ASSOCIATED CONTENT

Supporting Information

The Supporting Information is available free of charge on the ACS Publications website at DOI: 10.1021/acs.jpcc.6b08531.

Synthesis and characterization of dyes, calculated optimized molecular structure, molecular energy level diagram and relaxation processes, absorption spectra of the devices, electric dipole moment in the ground state, and HOMO and LUMO plots (PDF)

DOI: 10.1021/acs.jpcc.6b08531
J. Phys. Chem. C 2016, 120, 26206−26216

AUTHOR INFORMATION

Corresponding Authors

*E-mail: nohta@nctu.edu.tw. Tel.: +886 3 513 1395.
*E-mail: hirohiko-kono@m.tohoku.ac.jp. Tel.: +81 22 795 7720.

Notes

The authors declare no competing financial interest.

ACKNOWLEDGMENTS

N. O. thanks Professor Yuan-Pern Lee (National Chiao Tung University) for generous support. N. O., K. A., and E. W-G. D. are supported by National Chiao Tung University, Ministry of Science and Technology, and the MOE-ATU program of Taiwan. This work was also supported by Research Institute for Electronic Science at Hokkaido University, Japan. H. K. acknowledges Grant-in-Aid for Scientific Research by MEXT (No. 16H04091). K. N. thanks Institute for Quantum Chemical Exploration (IQCE) for financial support.

REFERENCES

(1) O'Regan, B.; Grätzel, M. A Low-Cost, High-Efficiency Solar Cell Based on Dye-Sensitized Colloidal TiO_2 Films. *Nature* **1991**, *353*, 737−740.
(2) Imahori, H.; Umeyama, T.; Ito, S. Large π-Aromatic Molecules as Potential Sensitizers for Highly Efficient Dye-Sensitized Solar Cells. *Acc. Chem. Res.* **2009**, *42*, 1809−1818.
(3) Hagfeldt, A.; Boschloo, G.; Sun, L.; Kloo, L.; Pettersson, H. Dye-Sensitized Solar Cells. *Chem. Rev.* **2010**, *110*, 6595−6663.
(4) Yella, A.; Lee, H.-W.; Tsao, H. N.; Yi, C.; Chandiran, A. K.; Nazeeruddin, M. K.; Diau, E. W.-G.; Yeh, C.-Y.; Zakeeruddin, S. M.; Grätzel, M. Porphyrin-Sensitized Solar Cells with Cobalt (II/III)-Based Redox Electrolyte Exceed 12% Efficiency. *Science* **2011**, *334*, 629−634.
(5) Li, L.-L.; Diau, E. W.-G. Porphyrin-Sensitized Solar Cells. *Chem. Soc. Rev.* **2013**, *42*, 291−304.
(6) Dou, L.; You, J.; Hong, Z.; Xu, Z.; Li, G.; Street, R. A.; Yang, Y. 25th Anniversary Article: A Decade of Organic/Polymeric Photovoltaic Research. *Adv. Mater.* **2013**, *25*, 6642−6670.
(7) Heeger, A. J. 25th Anniversary Article: Bulk Heterojunction Solar Cells: Understanding the Mechanism of Operation. *Adv. Mater.* **2014**, *26*, 10−27.
(8) Krebs, F. C.; Espinosa, N.; Hösel, M.; Søndergaard, R. R.; Jørgensen, M. 25th Anniversary Article: Rise to Power-OPV-Based Solar Parks. *Adv. Mater.* **2014**, *26*, 29−38.
(9) Etxebarria, I.; Ajuria, J.; Pacios, R. Solution-Processable Polymeric Solar Cells: A Review on Materials, Strategies and Cell Architectures to Overcome 10%. *Org. Electron.* **2015**, *19*, 34−60.
(10) Chang, J. A.; Rhee, J. H.; Im, S. H.; Lee, Y. H.; Kim, H.-j.; Seok, S. I.; Nazeeruddin, M. K.; Gratzel, M. High-Performance Nanostructured Inorganic-Organic Heterojunction Solar Cells. *Nano Lett.* **2010**, *10*, 2609−2612.
(11) Lee, J.-W.; Son, D.-Y.; Ahn, T. K.; Shin, H.-W.; Kim, I. Y.; Hwang, S.-J.; Ko, M. J.; Sul, S.; Han, H.; Park, N.-G. Quantum-Dot-Sensitized Solar Cell with Unprecedentedly High Photocurrent. *Sci. Rep.* **2013**, *3*, 1050.
(12) Christians, J. A.; Kamat, P. V. Trap and Transfer. Two-Step Hole Injection Across the Sb_2S_3/CuSCN Interface in Solid-State Solar Cells. *ACS Nano* **2013**, *7*, 7967−7974.
(13) Rhee, J. H.; Chung, C.-C.; Diau, E. W.-G. A Perspective of Mesoscopic Solar Cells Based on Metal Chalcogenide Quantum Dots and Organometal-Halide Perovskites. *NPG Asia Mater.* **2013**, *5*, e68.
(14) Kim, H.-S.; Lee, C.-R.; Im, J.-H.; Lee, K.-B.; Moehl, T.; Marchioro, A.; Moon, S.-J.; Humphry-Baker, R.; Yum, J.-H.; Moser, J. E.; Grätzel, M.; Park, N.-G. Lead Iodide Perovskite Sensitized All-Solid-State Submicron Thin Film Mesoscopic Solar Cell with Efficiency Exceeding 9%. *Sci. Rep.* **2012**, *2*, 591.
(15) Lee, M. M.; Teuscher, J.; Miyasaka, T.; Murakami, T. N.; Snaith, H. J. Efficient Hybrid Solar Cells Based on Meso-Superstructured Organometal Halide Perovskites. *Science* **2012**, *338*, 643−647.
(16) Liu, M.; Johnston, M. B.; Snaith, H. J. Efficient Planar Heterojunction Perovskite Solar Cells by Vapour Deposition. *Nature* **2013**, *501*, 395−398.
(17) Zhou, H.; Chen, Q.; Li, G.; Luo, S.; Song, T.-b.; Duan, H.-S.; Hong, Z.; You, J.; Liu, Y.; Yang, Y. Interface Engineering of Highly Efficient Perovskite Solar Cells. *Science* **2014**, *345*, 542−546.
(18) Yang, W. S.; Noh, J. H.; Jeon, N. J.; Kim, Y. C.; Ryu, S.; Seo, J.; Seok, S. I. High-Performance Photovoltaic Perovskite Layers Fabricated Through Intramolecular Exchange. *Science* **2015**, *348*, 1234−1237.
(19) Chan, C.-Y.; Wang, Y.; Wu, G.-W.; Diau, E. W.-G. Solvent-Extraction Crystal Growth for Highly Efficient Carbon-Based Mesoscopic Perovskite Solar Cells Free of Hole Conductors. *J. Mater. Chem. A* **2016**, *4*, 3872−3878.
(20) Hsu, H.-Y.; Chiang, H.-C.; Hu, J.-Y.; Awasthi, K.; Mai, C.-L.; Yeh, C.-Y.; Ohta, N.; Diau, E. W.-G. Field-Induced Fluorescence Quenching and Enhancement of Porphyrin Sensitizers on TiO_2 Films and in PMMA Films. *J. Phys. Chem. C* **2013**, *117*, 24761−24766.
(21) Leijtens, T.; Kandada, A. R. S.; Eperon, G. E.; Grancini, G.; D'Innocenzo, V.; Ball, J. M.; Stranks, S. D.; Snaith, H. J.; Petrozza, A. Modulating the Electron-Hole Interaction in a Hybrid Lead Halide Perovskite with an Electric Field. *J. Am. Chem. Soc.* **2015**, *137*, 15451−15459.
(22) Ardo, S.; Sun, Y.; Castellano, F. N.; Meyer, G. J. Excited-State Electron Transfer from Ruthenium-Polypyridyl Compounds to Anatase TiO_2 Nanocrystallites: Evidence for a Stark Effect. *J. Phys. Chem. B* **2010**, *114*, 14596−14604.
(23) Pastore, M.; Angelis, F. D. Computational Modeling of Stark Effects in Organic Dye-Sensitized TiO_2 Heterointerfaces. *J. Phys. Chem. Lett.* **2011**, *2*, 1261−1267.
(24) Cappel, U. B.; Feldt, S. M.; Schöneboom, J.; Hagfeldt, A.; Boschloo, G. The Influence of Local Electric Fields on Photoinduced Absorption in Dye-Sensitized Solar Cells. *J. Am. Chem. Soc.* **2010**, *132*, 9096−9101.
(25) Horiuchi, T.; Miura, H.; Sumioka, K.; Uchida, S. High Efficiency of Dye-Sensitized Solar Cells Based on Metal-Free Indoline Dyes. *J. Am. Chem. Soc.* **2004**, *126*, 12218−12219.
(26) Ito, S.; Miura, H.; Uchida, S.; Takata, M.; Sumioka, K.; Liska, P.; Comte, P.; Pechy, P.; Grätzel, M. High-Conversion-Efficiency Organic Dye-Sensitized Solar Cells with a Novel Indoline Dye. *Chem. Commun.* **2008**, 5194−5196.
(27) Higashijima, S.; Miura, H.; Fujita, T.; Kubota, Y.; Funabiki, K.; Yoshida, T.; Matsui, M. Highly Efficient New Indoline Dye Having Strong Electron-Withdrawing Group for Zinc Oxide Dye-Sensitized Solar Cell. *Tetrahedron* **2011**, *67*, 6289−6293.
(28) Higashijima, S.; Inoue, Y.; Miura, H.; Kubota, Y.; Funabiki, K.; Yoshida, T.; Matsui, M. Organic Dyes Containing Fluorene-Substituted Indoline Core for Zinc Oxide Dye-Sensitized Solar Cell. *RSC Adv.* **2012**, *2*, 2721−2724.
(29) Shibayama, N.; Inoue, Y.; Abe, M.; Kajiyama, S.; Ozawa, H.; Miura, H.; Arakawa, H. Novel Near-Infrared Carboxylated 1,3-Indandione Sensitizers for Highly Efficient Flexible Dye-Sensitized Solar Cells. *Chem. Commun.* **2015**, *51*, 12795−12798.
(30) Umeuchi, S.; Nishimura, Y.; Yamazaki, I.; Murakami, H.; Yamashita, M.; Ohta, N. Electric Field Effects on Absorption and Fluorescence Spectra of Pyrene Doped in a PMMA Polymer Film. *Thin Solid Films* **1997**, *311*, 239−245.
(31) Mehata, M. S.; Hsu, C.-S.; Lee, Y.-P.; Ohta, N. Electric Field Effects on Photoluminescence of Polyfluorene Thin Films: Dependence on Excitation Wavelength, Field Strength, and Temperature. *J. Phys. Chem. C* **2009**, *113*, 11907−11915.
(32) Tsushima, M.; Ushizaka, T.; Ohta, N. Time-Resolved Measurement System of Electrofluorescence Spectra. *Rev. Sci. Instrum.* **2004**, *75*, 479−485.
(33) Matsui, M.; Tanaka, N.; Kubota, Y.; Funabiki, K.; Jin, J.; Higashijima, S.; Miura, H.; Manseki, K. Long-Term Stability of Novel

DOI: 10.1021/acs.jpcc.6b08531
J. Phys. Chem. C 2016, 120, 26206−26216

Double Rhodanine Indoline Dyes Having One and Two Anchor Carboxyl Group(s) in Dye-Sensitized Solar Cells. *RSC Adv.* **2016**, *6*, 33111−33119.
(34) Nazeeruddin, M. K.; Kay, A.; Rodicio, I.; Humphry-Baker, R.; Müller, E.; Liska, P.; Vlachopoulos, N.; Grätzel, M. Conversion of Light to Electricity by *cis*-X_2Bis(2,2′-bipyridyl-4,4′-dicarboxylate)-ruthenium(II) Charge-Transfer Sensitizers (X = Cl^-, Br^-, I^-, CN^-, and SCN^-) on Nanocrystalline TiO_2 Electrodes. *J. Am. Chem. Soc.* **1993**, *115*, 6382−6390.
(35) Frisch, M. J.; Trucks, G. W.; Schlegel, H. B.; Scuseria, G. E.; Robb, M. A.; Cheeseman, J. R.; Scalmani, G.; Barone, V.; Mennucci, B.; Petersson, G. A. et al. *Gaussian 09*, Revision A.02; Gaussian, Inc.: Wallingford CT, 2009.
(36) Becke, A. D. Density-Functional Thermochemistry. III. The Role of Exact Exchange. *J. Chem. Phys.* **1993**, *98*, 5648−5652.
(37) Liptay, W. In *Excited States*; Lim, E. C., Ed.; Academic Press: New York, 1974; Vol.*1*, pp 129−229.
(38) Bublitz, G. U.; Boxer, S. G. Stark Spectroscopy: Applications in Chemistry, Biology, and Materials Science. *Annu. Rev. Phys. Chem.* **1997**, *48*, 213−242.
(39) Locknar, S. A.; Peteanu, L. A. Investigation of the Relationship between Dipolar Properties and Cis-Trans Configuration in Retinal Polyenes: A Comparative Study Using Stark Spectroscopy and Semiempirical Calculations. *J. Phys. Chem. B* **1998**, *102*, 4240−4246.
(40) Vance, F. W.; Williams, R. D.; Hupp, J. T. Electroabsorption Spectroscopy of Molecular Inorganic Compounds. *Int. Rev. Phys. Chem.* **1998**, *17*, 307−329.
(41) Ohta, N. Electric Field Effects on Photochemical Dynamics in Solid Films. *Bull. Chem. Soc. Jpn.* **2002**, *75*, 1637−1655.
(42) Jalviste, E.; Ohta, N. Theoretical Foundation of Electro-absorption Spectroscopy: Self-Contained Derivation of the Basic Equations with the Direction Cosine Method and the Euler Angle Method. *J. Photochem. Photobiol., C* **2007**, *8*, 30−46.
(43) Chowdhury, A.; Locknar, S. A.; Premvardhan, L. L.; Peteanu, L. A. Effects of Matrix Temperature and Rigidity on the Electronic Properties of Solvatochromic Molecules: Electroabsorption of Coumarin 153. *J. Phys. Chem. A* **1999**, *103*, 9614−9625.
(44) Legaspi, C. M.; Peteanu, L. A.; Yaron, D. J. Modeling Field-Induced Quenching in Poly(*p*-phenylene vinylene) Polymers and Oligomers. *J. Phys. Chem. B* **2015**, *119*, 7625−7634.

DOI: 10.1021/acs.jpcc.6b08531
J. Phys. Chem. C 2016, 120, 26206−26216